

How transverse momentum conservation breaks azimuthal correlation factorization

Jia-Lin Pei,^{1,2} Guo-Liang Ma,^{1,2,*} and Adam Bzdak^{3,†}

¹*Key Laboratory of Nuclear Physics and Ion-beam Application (MOE), Institute of Modern Physics, Fudan University, Shanghai 200433, China*

²*Shanghai Research Center for Theoretical Nuclear Physics, NSFC and Fudan University, Shanghai 200438, China*

³*AGH University of Krakow,*

Faculty of Physics and Applied Computer Science, 30-059 Kraków, Poland

The breakdown of azimuthal two-particle correlation factorization, quantified by the ratios r_2 and r_3 , serves as a sensitive probe of transverse-momentum-dependent flow fluctuations. While hydrodynamic models predict $r_3 \leq 1$, experimental data from CMS in p-Pb collisions exhibit $r_3 > 1$, presenting a clear puzzle. We show that transverse momentum conservation (TMC) is the key mechanism dictating this factorization breakdown in small systems. We systematically calculate the effect of TMC as a function of the momentum difference between particles across various multiplicity and momentum ranges. Our results are in quantitative agreement with CMS p-Pb data for both r_2 and r_3 . A central finding is a sign rule: under TMC, the deviation $r_n - 1$ follows $(-1)^{n+1}$, being negative for even and positive for odd harmonic orders n . This work establishes an analytical framework to quantify transverse-momentum-dependent flow fluctuations and provides new insights into the origin of collectivity in small colliding systems.

I. INTRODUCTION

The quark-gluon plasma (QGP), a deconfined state of quarks and gluons governed by Quantum Chromodynamics (QCD) under conditions of extreme temperature and density, is the primary object of study in ultra-relativistic heavy-ion collisions at the BNL Relativistic Heavy Ion Collider (RHIC) and the CERN Large Hadron Collider (LHC) [1–5]. Among the most powerful signatures of this state is the azimuthal anisotropy of particle emission in the transverse plane [6–9]. The initial geometric asymmetries and energy-density inhomogeneities are mapped, via the collective evolution of the QGP, into momentum anisotropies imprinted on final-state particles, a phenomenon referred to as collective flow [10, 11]. This evolution is successfully described by both relativistic hydrodynamic models [11, 12] and transport models [13]. Motivated by such models, this anisotropy is quantified by a Fourier expansion of the azimuthal angle (ϕ) distribution of emitted particles [14–16],

$$\frac{dN}{d\phi} \propto 1 + 2 \sum_n v_n \cos[n(\phi - \Psi_n)]. \quad (1)$$

Here, the Fourier coefficient v_n and the event plane angle Ψ_n represent the magnitude and orientation, respectively, of the n^{th} -order harmonic flow vector $\vec{V}_n = v_n e^{in\Psi_n}$. Typically, the most significant flow coefficient corresponds to the elliptic flow v_2 , resulting from the initial almond-shaped overlap region in noncentral collisions. However, positional fluctuations of both the colliding nuclei and the nucleons within them can lead to more complex geometric configurations or higher-order eccentricities ε_n of the initial geometry, thereby resulting in non-vanishing flow coefficients v_n for $n > 2$, such as the triangular flow v_3 [17–20]. The event-plane angle Ψ_n is determined by the n^{th} -order participant-plane angle of the initial nucleon overlap region, which fluctuates event-by-event due to the varying spatial distribution of participating nucleons [17]. The azimuthal anisotropies serve as powerful probes for constraining the initial state of heavy-ion collisions and quantifying certain transport properties of the QGP, e.g., the ratio of shear viscosity to entropy density, η/s [21–24]. Comparisons with theoretical models have revealed that the QGP behaves as a nearly perfect fluid, with a shear viscosity to entropy density ratio η/s close to the quantum lower bound of $1/(4\pi)$. This low value signals extremely strong interactions among its constituents inside the QGP [25–27].

A standard experimental method determines the single-particle flow harmonic v_n by measuring two-particle azimuthal correlations, avoiding the uncertainties associated with event-plane estimation [28]. The two-particle distri-

*Electronic address: glma@fudan.edu.cn

†Electronic address: bzdak@fis.agh.edu.pl

bution in relative azimuthal angle $\Delta\phi = \phi^a - \phi^b$ can be expressed as a Fourier series [14, 15],

$$\frac{dN^{\text{pair}}}{d\Delta\phi} \propto 1 + 2 \sum_n V_{n\Delta} \cos[n(\phi^a - \phi^b)]. \quad (2)$$

If collective flow serves as the primary source of final-state particle correlations, the factorization of the two-particle correlation $V_{n\Delta}$ can be characterized as,

$$V_{n\Delta}(p_T^a, p_T^b) = v_n(p_T^a) v_n(p_T^b), \quad (3)$$

where $v_n(p_T^a)$ and $v_n(p_T^b)$ represent the single-particle flow coefficients for a pair of particles with transverse momenta p_T^a and p_T^b , respectively. Thus, the p_T -dependent behavior of the single-particle v_n can be derived by fixing one particle within a relatively wide p_T interval, adjusting only the p_T of the other particle, and measuring $V_{n\Delta}$. The validity of Eq. (3) requires the condition $\Psi_n(p_T^a) = \Psi_n(p_T^b) = \Psi_n$, whereby the common event-plane angle cancels in two-particle correlations. However, research findings have shown that in the most central Pb-Pb collisions, the factorization assumption of Eq. (3) does not hold, with the degree of deviation reaching up to 20% [29]. This is primarily attributed to the presence of local fluctuations in the energy density within the overlapping region of two nuclei at the initial stage of collisions, a feature highlighted by hydrodynamic models. The p_T -differential impact of these fluctuations on particle emission causes the event plane to fluctuate across p_T ranges [30, 31], thereby modifying Eq. (3) as follows,

$$V_{n\Delta}(p_T^a, p_T^b) = v_n(p_T^a) v_n(p_T^b) \cos[n(\Psi(p_T^a) - \Psi(p_T^b))]. \quad (4)$$

Thus, Eq. (4) implies a p_T -dependent factorization breaking of Eq. (3), with the factorization ratio r_n (defined in Sec. II) of $\cos[n(\Psi(p_T^a) - \Psi(p_T^b))]$. This provides a unique probe into the fluctuations in the initial state of heavy ion collisions along the radial direction.

In contrast to large A+A systems, the origin of azimuthal particle correlations in small systems ($p+p$ and $p+A$) remains an open and vital question. The theoretical landscape for explaining azimuthal particle correlations in small systems comprises competing paradigms, including the color glass condensation (CGC) models [32–34], hydrodynamic models [35–37], and transport models like AMPT [38–40]. The observed factorization breakdown also serves as a critical test for the origin(s) of azimuthal correlations in small systems, because if such effects arise from hydrodynamics, hydrodynamic models must account for the experimental data. The factorization ratios r_n for $V_{n\Delta}$ ($n=2$ and 3), to be defined in Eq. (9), have been measured in p-Pb collisions by the CMS collaboration [41]. For the elliptic harmonic ($V_{2\Delta}$), hydrodynamic simulations with MC-Glauber initial conditions can approximately describe the data, where the measured factorization ratio r_2 falls below unity at low multiplicity and high p_T . In contrast, the triangular harmonic ($V_{3\Delta}$) exhibits a ratio r_3 that exceeds unity in the same kinematic region, incompatible with hydrodynamic calculations which predict $r_3 \leq 1$. This discrepancy demonstrates that hydrodynamic models cannot simultaneously describe the factorization patterns of both r_2 and r_3 in small systems. In addition, a systematic study of p_T -dependent flow vector fluctuations within the AMPT model demonstrated that the factorization breaking of $V_{2\Delta}$ is highly sensitive to changes in initial conditions but exhibits negligible dependence on the parton cross-section and hadronic rescatterings [42]. This underscores the need to explore the mechanisms for factorization breaking, as precision studies of this phenomenon in small systems will thus be helpful for understanding the origin(s) of azimuthal particle correlations in small systems [43].

Transverse momentum conservation (TMC) imposes an inherent constraint on final-state momentum distributions, generating significant azimuthal correlations that are particularly important in low-multiplicity small systems [44–46]. Our earlier work has shown that the interplay between the TMC and collective flow can describe a range of observed correlations in small systems [47–51]. In this paper, we calculate the factorization breakdown of $V_{2\Delta}$ and $V_{3\Delta}$ based on the TMC framework. We compare our analytical calculations with CMS p-Pb data [41] to explore the mechanisms driving azimuthal particle correlations in small systems.

II. FACTORIZATION RATIOS FROM TMC AND FLOW

The observable used to study p_T -dependent flow vector fluctuations is the factorization ratio r_n , which is defined via two-particle harmonic flows and used to probe the factorization of two particles in different p_T intervals. Its definition is given by [52],

$$r_n = \frac{V_{n\Delta}(p_T^a, p_T^b)}{\sqrt{V_{n\Delta}(p_T^a, p_T^a) V_{n\Delta}(p_T^b, p_T^b)}}, \quad (5)$$

where

$$V_{n\Delta}(p_T^a, p_T^b) = \left\langle e^{in(\phi_1^a - \phi_2^b)} \right\rangle = \langle \cos[n(\phi_1^a - \phi_2^b)] \rangle, \quad (6)$$

and the denominator represents the scenario where two particles originate from the same p_T interval, i.e.

$$V_{n\Delta}(p_T^a, p_T^a) = \left\langle e^{in(\phi_1^a - \phi_2^a)} \right\rangle = \langle \cos[n(\phi_1^a - \phi_2^a)] \rangle = v_n (p_T^a)^2, \quad (7)$$

$$V_{n\Delta}(p_T^b, p_T^b) = \left\langle e^{in(\phi_1^b - \phi_2^b)} \right\rangle = \langle \cos[n(\phi_1^b - \phi_2^b)] \rangle = v_n (p_T^b)^2. \quad (8)$$

If collective flow dominates and non-flow effects are negligible, Eq. (5) will be equivalent to the following formula,

$$r_n = \frac{v_n (p_T^a) v_n (p_T^b) \cos [n(\Psi_n(p_T^a) - \Psi_n(p_T^b))]}{\sqrt{v_n (p_T^a)^2 v_n (p_T^b)^2}}. \quad (9)$$

Consequently, the Cauchy-Schwarz inequality gives $r_n \leq 1$ for the factorization ratio defined in Eq. (9) [53].

A. TMC calculations

Consider a collision producing a total of N particles, with their individual transverse momenta being $\vec{p}_1, \vec{p}_2, \dots, \vec{p}_N$. Under the constraint of transverse momentum conservation, the transverse momentum distribution (normalized to unity) f_N of these N particles can be described as [48, 54–56]

$$f_N(\vec{p}_1, \vec{p}_2, \dots, \vec{p}_N) = \frac{\delta^2(\vec{p}_1 + \vec{p}_2 + \dots + \vec{p}_N) \prod_{i=1}^N f(\vec{p}_i)}{\int_F \delta^2(\vec{p}_1 + \vec{p}_2 + \dots + \vec{p}_N) \prod_{i=1}^N [f(\vec{p}_i) d^2 \vec{p}_i]}, \quad (10)$$

where the δ function constitutes the mathematical expression of TMC, $f(\vec{p}_i)$ is the normalized single-particle distribution, and it is assumed here that all particles follow the same transverse momentum distribution; F denotes the full phase space. To calculate two-particle azimuthal correlation function such as $\langle \cos[n(\phi_1 - \phi_2)] \rangle$, it is necessary to know the two-particle distribution function f_2 , which can be obtained by integrating out the momenta of the remaining $N - 2$ particles in Eq. (10),

$$f_2(\vec{p}_1, \vec{p}_2) = f(\vec{p}_1) f(\vec{p}_2) \frac{\int_F \delta^2(\vec{p}_1 + \vec{p}_2 + \dots + \vec{p}_N) \prod_{i=3}^N [f(\vec{p}_i) d^2 \vec{p}_i]}{\int_F \delta^2(\vec{p}_1 + \vec{p}_2 + \dots + \vec{p}_N) \prod_{i=1}^N [f(\vec{p}_i) d^2 \vec{p}_i]}. \quad (11)$$

To evaluate the integral in Eq. (11), we define the sum of the transverse momenta of M particles as $\vec{K} \equiv \sum_{i=1}^M \vec{p}_i$. According to the central limit theorem, \vec{K} satisfies a Gaussian distribution, i.e.,

$$G_M(\vec{K}) \equiv \int_F \delta^2 \left(-\vec{K} + \sum_{i=1}^M \vec{p}_i \right) \prod_{i=1}^M (f(\vec{p}_i) d^2 \vec{p}_i) = \frac{1}{\pi \sigma^2} \exp \left(-\frac{|\vec{K}|^2}{\sigma^2} \right), \quad (12)$$

where the mean and variance of \vec{K} are as follows:

$$\begin{aligned} \left\langle \vec{K} \right\rangle_F &= \left\langle \sum_{i=1}^M \vec{p}_i \right\rangle_F = \sum_{i=1}^M \langle \vec{p}_i \rangle_F = 0, \\ \sigma^2 &= M \left(\left\langle |\vec{p}|^2 \right\rangle_F - \langle \vec{p} \rangle_F^2 \right) = M \left\langle |\vec{p}|^2 \right\rangle_F, \end{aligned} \quad (13)$$

and

$$\left\langle |\vec{p}|^2 \right\rangle_F = \frac{\int_F |\vec{p}|^2 f(\vec{p}) d^2 \vec{p}}{\int_F f(\vec{p}) d^2 \vec{p}}. \quad (14)$$

Therefore, in accordance with Eq. (12), Eq. (11) can be further described as follows:

$$f_2(\vec{p}_1, \vec{p}_2) = f(\vec{p}_1)f(\vec{p}_2) \frac{G_{N-2}(-\vec{p}_1 - \vec{p}_2)}{G_N(0)} = f(\vec{p}_1)f(\vec{p}_2) \frac{N}{N-2} \exp\left(-\frac{(\vec{p}_1 + \vec{p}_2)^2}{(N-2)\langle|\vec{p}|^2\rangle_F}\right). \quad (15)$$

It can be seen from Eq. (15) that the two-particle density distribution f_2 depends on the sum of the transverse momentum vectors, and thus reaches its maximum value in the back-to-back configuration. In addition, we also need to specify the form of the single-particle distribution, which is generally determined as follows:

$$f(\vec{p}) = \frac{g(p)}{2\pi} (1 + 2v_2(p) \cos[2(\phi - \Psi_2(p))]). \quad (16)$$

By combining Eq. (16), Eq. (15) can be fully expressed as:

$$\begin{aligned} f_2(\vec{p}_1, \vec{p}_2) &= \frac{g(p_1)}{2\pi} \frac{g(p_2)}{2\pi} (1 + 2v_2(p_1) \cos[2(\phi_1 - \Psi_2(p_1))]) (1 + 2v_2(p_2) \cos[2(\phi_2 - \Psi_2(p_2))]) \\ &\times \frac{N}{N-2} \exp\left(-\frac{(p_{1,x} + p_{2,x})^2}{2(N-2)\langle p_x^2 \rangle_F} - \frac{(p_{1,y} + p_{2,y})^2}{2(N-2)\langle p_y^2 \rangle_F}\right), \end{aligned} \quad (17)$$

where

$$p_x = p \cos(\phi), \quad p_y = p \sin(\phi), \quad (18)$$

$$\langle p_x^2 \rangle_F = \frac{1}{2} \langle p^2 \rangle_F (1 + v_{2F}), \quad \langle p_y^2 \rangle_F = \frac{1}{2} \langle p^2 \rangle_F (1 - v_{2F}), \quad (19)$$

$$v_{2F} = \frac{\int_F v_2(p) g(p) \cos[2\Psi_2(p)] p^2 d^2p}{\int_F g(p) p^2 d^2p}. \quad (20)$$

Based on Eq. (17), we can calculate various types of two-particle azimuthal correlations under a given transverse momentum, such as r_2 and r_3 in Eq. (5),

$$r_2 = \frac{\langle \cos[2(\phi_1^a - \phi_2^b)] \rangle}{\sqrt{\langle \cos[2(\phi_1^a - \phi_2^a)] \rangle \langle \cos[2(\phi_1^b - \phi_2^b)] \rangle}}, \quad r_3 = \frac{\langle \cos[3(\phi_1^a - \phi_2^b)] \rangle}{\sqrt{\langle \cos[3(\phi_1^a - \phi_2^a)] \rangle \langle \cos[3(\phi_1^b - \phi_2^b)] \rangle}}. \quad (21)$$

Taking the numerator of r_2 in Eq. (21) as an example, its calculation process and result are as follows:

$$\begin{aligned} \langle \cos[2(\phi_1^a - \phi_2^b)] \rangle | p_a, p_b &= \frac{\int_0^{2\pi} \cos[2(\phi_1^a - \phi_2^b)] f_2(p_a, \phi_1^a, p_b, \phi_2^b) d\phi_1^a d\phi_2^b}{\int_0^{2\pi} f_2(p_a, \phi_1^a, p_b, \phi_2^b) d\phi_1^a d\phi_2^b} \\ &\approx A_0 + A_1 Y_A + \frac{1}{2} A_2 Y_A^2, \end{aligned} \quad (22)$$

where

$$Y_A = -\frac{1}{(N-2)\langle p^2 \rangle_F}, \quad (23)$$

and

$$\begin{aligned} A_0 &= v_2(p_a)v_2(p_b) \cos[2\Psi_2(p_a) - 2\Psi_2(p_b)], \\ A_1 &= -\frac{1}{2} p_b^2 v_{2F} v_2(p_a) \cos[2\Psi_2(p_a)] + p_a^2 v_2(p_a)v_2(p_b) \cos[2\Psi_2(p_a) - 2\Psi_2(p_b)] \\ &\quad + p_b^2 v_2(p_a)v_2(p_b) \cos[2\Psi_2(p_a) - 2\Psi_2(p_b)] - \frac{1}{2} p_a^2 v_{2F} v_2(p_b) \cos[2\Psi_2(p_b)], \\ A_2 &= p_a^2 p_b^2 + \frac{1}{2} p_a^2 p_b^2 v_{2F}^2 - 3p_a^2 p_b^2 v_{2F} v_2(p_a) \cos[2\Psi_2(p_a)] - p_b^4 v_{2F} v_2(p_a) \cos[2\Psi_2(p_a)] \end{aligned}$$

$$\begin{aligned}
& + p_a^4 v_2(p_a) v_2(p_b) \cos[2\Psi_2(p_a) - 2\Psi_2(p_b)] + 4p_a^2 p_b^2 v_2(p_a) v_2(p_b) \cos[2\Psi_2(p_a) - 2\Psi_2(p_b)] \\
& + p_b^4 v_2(p_a) v_2(p_b) \cos[2\Psi_2(p_a) - 2\Psi_2(p_b)] + \frac{1}{2} p_a^4 v_{2F}^2 v_2(p_a) v_2(p_b) \cos[2\Psi_2(p_a) - 2\Psi_2(p_b)] \\
& + 2p_a^2 p_b^2 v_{2F}^2 v_2(p_a) v_2(p_b) \cos[2\Psi_2(p_a) - 2\Psi_2(p_b)] + \frac{1}{2} p_b^4 v_{2F}^2 v_2(p_a) v_2(p_b) \cos[2\Psi_2(p_a) - 2\Psi_2(p_b)] \\
& - p_a^4 v_{2F} v_2(p_b) \cos[2\Psi_2(p_b)] - 3p_a^2 p_b^2 v_{2F} v_2(p_b) \cos[2\Psi_2(p_b)] + \frac{1}{4} p_a^4 v_{2F}^2 v_2(p_a) v_2(p_b) \cos[2\Psi_2(p_a) + 2\Psi_2(p_b)] \\
& + \frac{1}{4} p_b^4 v_{2F}^2 v_2(p_a) v_2(p_b) \cos[2\Psi_2(p_a) + 2\Psi_2(p_b)]. \tag{24}
\end{aligned}$$

The above results are based on the expansion of the exponential term in Eq. (17) to the second order, i.e., $\exp(-X) \approx 1 - X + \frac{X^2}{2}$, since the first non-vanishing pure TMC term, i.e., the first term of A_2 in Eq. (24), appears at $\frac{X^2}{2}$. For the denominator of Eq. (22), we only take the first term of its expansion, so the result is $(2\pi)^2$. Here “pure TMC” refers to the terms that depend only on N and p , “pure flow” refers to the terms that depend only on v_n and Ψ_n , and “interplay” between pure TMC and pure flow refers to the terms that depend on both N , p , v_n , Ψ_n in Eq. (24). In principle, we should also include v_3 in the above calculations; however, we verified that its contribution is negligible.

For the denominator of r_2 in Eq. (21), each factor under the square root corresponds to evaluating Eqs. (22) and (24) with both p_a and p_b uniformly set to p_a or to p_b , respectively.

Similarly, for the numerator of r_3 in Eq. (21), we obtain:

$$\begin{aligned}
\langle \cos[3(\phi_1^a - \phi_2^b)] \rangle | p_a, p_b &= \frac{\int_0^{2\pi} \cos[3(\phi_1^a - \phi_2^b)] f_2(p_a, \phi_1^a, p_b, \phi_2^b) d\phi_1^a d\phi_2^b}{\int_0^{2\pi} f_2(p_a, \phi_1^a, p_b, \phi_2^b) d\phi_1^a d\phi_2^b} \\
&\approx B_0 + B_1 Y_B + \frac{1}{2} B_2 Y_B^2 + \frac{1}{6} B_3 Y_B^3, \tag{25}
\end{aligned}$$

where

$$Y_B = -\frac{1}{(N-2) \langle p^2 \rangle_F}, \tag{26}$$

$$\begin{aligned}
f_2(p_a, \phi_1^a, p_b, \phi_2^b) &= \frac{g(p_a)}{2\pi} \frac{g(p_b)}{2\pi} (1 + 2v_2(p_a) \cos[2(\phi_1^a - \Psi_2(p_a))] + 2v_3(p_a) \cos[3(\phi_1^a - \Psi_3(p_a))]) \\
&\quad \times (1 + 2v_2(p_b) \cos[2(\phi_2^b - \Psi_2(p_b))] + 2v_3(p_b) \cos[3(\phi_2^b - \Psi_3(p_b))]) \\
&\quad \times \frac{N}{N-2} \exp\left(-\frac{(p_{a,x} + p_{b,x})^2}{2(N-2) \langle p_x^2 \rangle_F} - \frac{(p_{a,y} + p_{b,y})^2}{2(N-2) \langle p_y^2 \rangle_F}\right), \tag{27}
\end{aligned}$$

and

$$\begin{aligned}
B_0 &= v_3(p_a) v_3(p_b) \cos[3\Psi_3(p_a) - 3\Psi_3(p_b)], \\
B_1 &= p_a p_b v_2(p_a) v_2(p_b) \cos[2\Psi_2(p_a) - 2\Psi_2(p_b)] + p_a^2 v_3(p_a) v_3(p_b) \cos[3\Psi_3(p_a) - 3\Psi_3(p_b)] \\
&\quad + p_b^2 v_3(p_a) v_3(p_b) \cos[3\Psi_3(p_a) - 3\Psi_3(p_b)], \\
B_2 &= -p_a p_b^3 v_{2F} v_2(p_a) \cos[2\Psi_2(p_a)] + 2p_a^3 p_b v_2(p_a) v_2(p_b) \cos[2\Psi_2(p_a) - 2\Psi_2(p_b)] \\
&\quad + 2p_a p_b^3 v_2(p_a) v_2(p_b) \cos[2\Psi_2(p_a) - 2\Psi_2(p_b)] + p_a^3 p_b v_{2F}^2 v_2(p_a) v_2(p_b) \cos[2\Psi_2(p_a) - 2\Psi_2(p_b)] \\
&\quad + p_a p_b^3 v_{2F}^2 v_2(p_a) v_2(p_b) \cos[2\Psi_2(p_a) - 2\Psi_2(p_b)] - p_a^3 p_b v_{2F} v_2(p_b) \cos[2\Psi_2(p_b)] \\
&\quad + p_a^4 v_3(p_a) v_3(p_b) \cos[3\Psi_3(p_a) - 3\Psi_3(p_b)] + 4p_a^2 p_b^2 v_3(p_a) v_3(p_b) \cos[3\Psi_3(p_a) - 3\Psi_3(p_b)] \\
&\quad + p_b^4 v_3(p_a) v_3(p_b) \cos[3\Psi_3(p_a) - 3\Psi_3(p_b)] + \frac{1}{2} p_a^4 v_{2F}^2 v_3(p_a) v_3(p_b) \cos[3\Psi_3(p_a) - 3\Psi_3(p_b)] \\
&\quad + 2p_a^2 p_b^2 v_{2F}^2 v_3(p_a) v_3(p_b) \cos[3\Psi_3(p_a) - 3\Psi_3(p_b)] + \frac{1}{2} p_b^4 v_{2F}^2 v_3(p_a) v_3(p_b) \cos[3\Psi_3(p_a) - 3\Psi_3(p_b)], \\
B_3 &= p_a^3 p_b^3 + \frac{3}{2} p_a^3 p_b^3 v_{2F}^2 - 6p_a^3 p_b^3 v_{2F} v_2(p_a) \cos[2\Psi_2(p_a)] - 3p_a p_b^5 v_{2F} v_2(p_a) \cos[2\Psi_2(p_a)] \\
&\quad - \frac{3}{2} p_a^3 p_b^3 v_{2F}^3 v_2(p_a) \cos[2\Psi_2(p_a)] - \frac{3}{4} p_a p_b^5 v_{2F}^3 v_2(p_a) \cos[2\Psi_2(p_a)] + 3p_a^5 p_b v_2(p_a) v_2(p_b) \cos[2\Psi_2(p_a) - 2\Psi_2(p_b)] \\
&\quad + 9p_a^3 p_b^3 v_2(p_a) v_2(p_b) \cos[2\Psi_2(p_a) - 2\Psi_2(p_b)] + 3p_a p_b^5 v_2(p_a) v_2(p_b) \cos[2\Psi_2(p_a) - 2\Psi_2(p_b)]
\end{aligned}$$

$$\begin{aligned}
& + \frac{9}{2} p_a^5 p_b v_{2F}^2 v_2(p_a) v_2(p_b) \cos [2\Psi_2(p_a) - 2\Psi_2(p_b)] + \frac{27}{2} p_a^3 p_b^3 v_{2F}^2 v_2(p_a) v_2(p_b) \cos [2\Psi_2(p_a) - 2\Psi_2(p_b)] \\
& + \frac{9}{2} p_a p_b^5 v_{2F}^2 v_2(p_a) v_2(p_b) \cos [2\Psi_2(p_a) - 2\Psi_2(p_b)] - 3 p_a^5 p_b v_{2F} v_2(p_b) \cos [2\Psi_2(p_b)] \\
& - 6 p_a^3 p_b^3 v_{2F} v_2(p_b) \cos [2\Psi_2(p_b)] - \frac{3}{4} p_a^5 p_b v_{2F}^3 v_2(p_b) \cos [2\Psi_2(p_b)] - \frac{3}{2} p_a^3 p_b^3 v_{2F}^3 v_2(p_b) \cos [2\Psi_2(p_b)] \\
& + \frac{3}{4} p_a^5 p_b v_{2F}^2 v_2(p_a) v_2(p_b) \cos [2\Psi_2(p_a) + 2\Psi_2(p_b)] + \frac{3}{4} p_a p_b^5 v_{2F}^2 v_2(p_a) v_2(p_b) \cos [2\Psi_2(p_a) + 2\Psi_2(p_b)] \\
& + p_a^6 v_3(p_a) v_3(p_b) \cos [3\Psi_3(p_a) - 3\Psi_3(p_b)] + 9 p_a^4 p_b^2 v_3(p_a) v_3(p_b) \cos [3\Psi_3(p_a) - 3\Psi_3(p_b)] \\
& + 9 p_a^2 p_b^4 v_3(p_a) v_3(p_b) \cos [3\Psi_3(p_a) - 3\Psi_3(p_b)] + p_b^6 v_3(p_a) v_3(p_b) \cos [3\Psi_3(p_a) - 3\Psi_3(p_b)] \\
& + \frac{3}{2} p_a^6 v_{2F}^2 v_3(p_a) v_3(p_b) \cos [3\Psi_3(p_a) - 3\Psi_3(p_b)] + \frac{27}{2} p_a^4 p_b^2 v_{2F}^2 v_3(p_a) v_3(p_b) \cos [3\Psi_3(p_a) - 3\Psi_3(p_b)] \\
& + \frac{27}{2} p_a^2 p_b^4 v_{2F}^2 v_3(p_a) v_3(p_b) \cos [3\Psi_3(p_a) - 3\Psi_3(p_b)] + \frac{3}{2} p_b^6 v_{2F}^2 v_3(p_a) v_3(p_b) \cos [3\Psi_3(p_a) - 3\Psi_3(p_b)] \\
& - \frac{1}{8} p_a^6 v_{2F}^3 v_3(p_a) v_3(p_b) \cos [3\Psi_3(p_a) + 3\Psi_3(p_b)] - \frac{1}{8} p_b^6 v_{2F}^3 v_3(p_a) v_3(p_b) \cos [3\Psi_3(p_a) + 3\Psi_3(p_b)]. \tag{28}
\end{aligned}$$

The above results are based on the expansion of the exponential term in Eq. (27) to the third order, i.e., $\exp(-X) \approx 1 - X + \frac{X^2}{2} - \frac{X^3}{6}$, since the first non-vanishing pure TMC term, i.e., the first term of B_3 in Eq. (28), appears at $\frac{X^3}{6}$. For the denominator of Eq. (25), we only take the first term of its expansion, so the result is $(2\pi)^2$.

For the denominator of r_3 in Eq. (21), each factor under the square root corresponds to evaluating Eqs. (25) and (28) with both p_a and p_b uniformly set to p_a or to p_b , respectively.

III. RESULTS AND DISCUSSION

A. Comparison with CMS data: r_2 and r_3

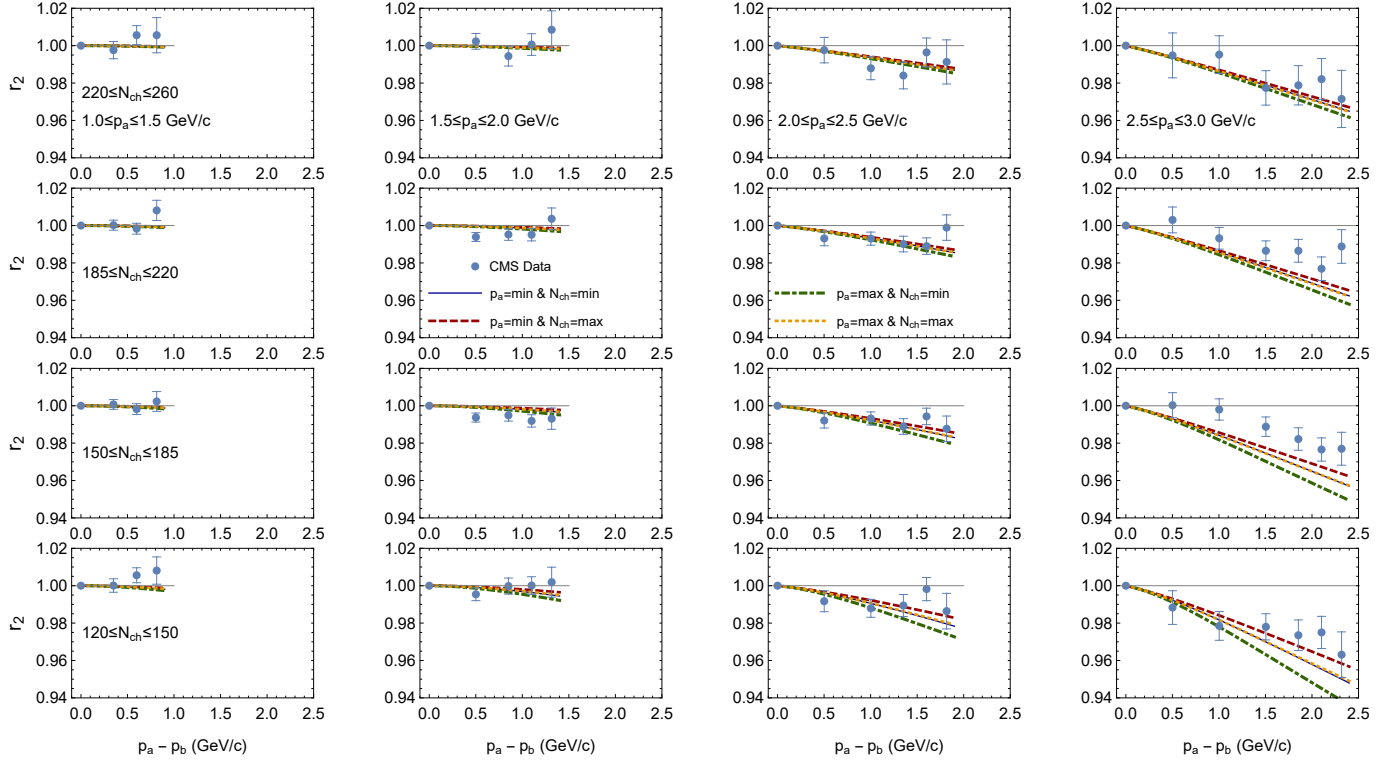


FIG. 1: Factorization ratio r_2 as a function of $p_a - p_b$ in four p_a bins (columns) and four N_{ch} ranges (rows), forming a 4×4 array of panels. Curves: TMC calculations. Points: CMS p-Pb data at 5.02 TeV with statistical errors (systematic uncertainties negligible) [41].

In Fig. 1, we present the calculated factorization ratio r_2 as a function of $p_a - p_b$ in four p_a bins and four N_{ch} ranges, compared with the CMS p-Pb data at 5.02 TeV. Using the extreme values of the p_a and N_{ch} ranges from the CMS cuts, we set four parameter combinations for p_a and N_{ch} (with $N = 1.5N_{ch}$) and calculate the corresponding theoretical curves via Eqs. (21) and (22), yielding four curves in each panel. The p -dependence of v_2 is extracted from fits to the measured v_2 {2} and v_2 {4} under the same experimental conditions [57] (see Appendix A for details). Our results are practically insensitive to the choice of v_{2F} , which we set to $v_{2F} = 0.025$. For $\langle p^2 \rangle_F$, we assume

$$f(p) \propto \exp\left(-\frac{p}{T}\right), \quad (29)$$

which gives $\langle p \rangle_F = 2T$ and $\langle p^2 \rangle_F = 6T^2$. According to Ref. [58], the value of $\langle p \rangle$ in p-Pb collisions at 5.02 TeV is approximately 0.78 GeV/c for high multiplicities, we then set $\langle p^2 \rangle_F = 0.91$ (GeV/c)². The correlations between event planes at different p in Eq. (24) are approximated by the experimental values shown in the first row of panels of Fig. 1. Since high-multiplicity p-Pb events are predominantly flow-driven, our analytical results converge to the form of Eq. (9). Consequently, r_2 reduces to $\cos[2\Psi_2(p_a) - 2\Psi_2(p_b)]$ in this limit (see Appendix B for details). In addition, we also present the results obtained without considering the p_T -dependent event plane fluctuations, i.e., setting $\cos[2\Psi_2(p_a) - 2\Psi_2(p_b)] = 1$, which serves to highlight the contribution of TMC more distinctly (see Appendix C for details). With the above parameter set, our calculated r_2 is found to be below unity and to decrease with increasing $p_a - p_b$, in good agreement with the CMS data for all studied kinematic cuts. The origin of $r_2 \leq 1$ lies in the TMC effect, which will be demonstrated and explained in Figs. 3 and 4 and the accompanying text. The factorization breaking effect strengthens progressively with decreasing multiplicity (top to bottom in each column) and increasing momentum (left to right in each row). This is consistent with the characteristic of the TMC effect being more significant at lower multiplicities and higher momenta. Thus, at lower multiplicities and higher momenta, factorization breaking is most pronounced for the green dash-dotted lines, and least for the red dashed ones. The blue

solid and orange dotted lines lie between these extremes, essentially overlapping. This underscores that the TMC effect must therefore be accounted for in interpreting r_2 , particularly at lower multiplicities and higher momenta.

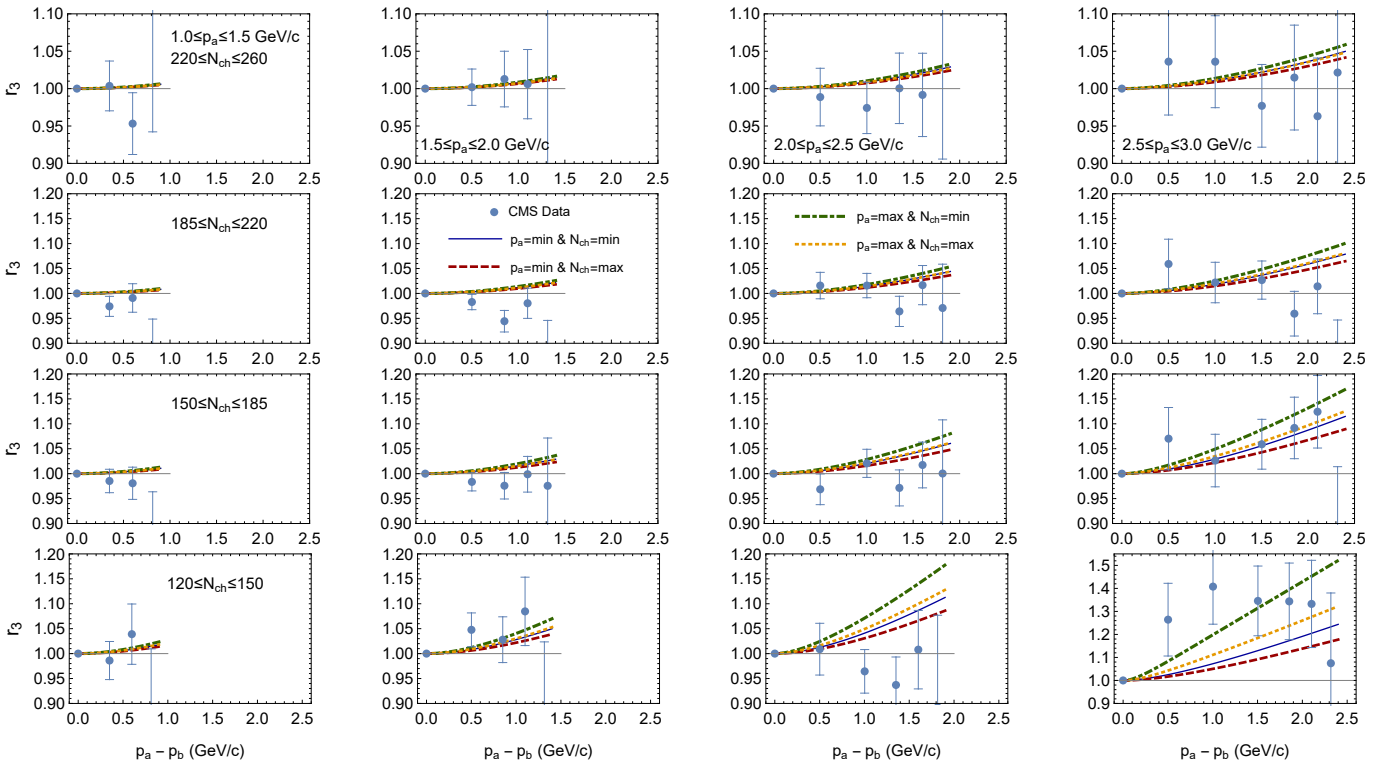


FIG. 2: Factorization ratio r_3 as a function of $p_a - p_b$ in four p_a bins (columns) and four N_{ch} ranges (rows), forming a 4×4 array of panels. Curves: TMC calculations. Points: CMS p-Pb data at 5.02 TeV with statistical errors (systematic uncertainties negligible) [41].

In Fig. 2, we present the calculated factorization ratio r_3 as a function of $p_a - p_b$ in four p_a bins and four N_{ch} ranges, compared with the CMS p-Pb data at 5.02 TeV, with all parameter settings consistent with those in Fig. 1. Following the same logic as for r_2 , r_3 should reduce to $\cos[3\Psi_3(p_a) - 3\Psi_3(p_b)]$ in high-multiplicity p-Pb events. However, as the experimental data in Fig. 2 (top row) are consistent with unity within uncertainties, we ignore in our analysis the p_T -dependent 3rd event-plane correlations in Eq. (28). For the second-order event plane that still appears in r_3 , its setting method is consistent with that of r_2 in Fig. 1. Furthermore, we also present the results of r_3 obtained without considering the p_T -dependent second-order event plane fluctuations and find that its effect is negligible (see Appendix C for details). We observe that $r_3 > 1$ emerges in our analysis, in sharp contrast to $r_2 < 1$ in Fig. 1. This is attributed to the TMC effect which is most evident at lower multiplicities and higher momenta. Figures 4 and 5 (and accompanying text) will reveal the mechanism by which the TMC effect drives r_3 above unity. Although r_3 and r_2 deviate from unity in opposite directions, the magnitude of deviation for both increases monotonically with $p_a - p_b$. Notably, r_3 exhibits a much stronger dependence on multiplicity than r_2 . If taking the last-column curves (e.g. the orange dotted lines) in Figs. 1 and 2 as an example, we observe that r_2 varies by only about 2% from top to bottom, whereas r_3 changes by about 20%. Our TMC-based calculations reproduce the experimental data within uncertainties, capturing both $r_3 > 1$ and its trends with p_a and multiplicity. These findings support TMC as the mechanism responsible for $r_3 > 1$ in lower-multiplicity p-Pb events.

B. The sign rule of r_n

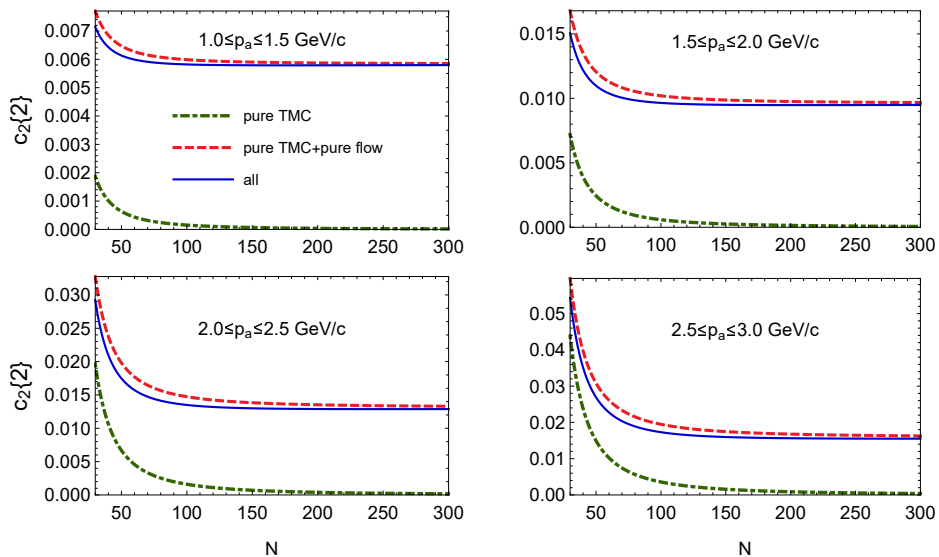


FIG. 3: $c_2\{2\}$ from “pure TMC”, “pure TMC+pure flow”, and “pure TMC+pure flow+interplay” (labeled as “all”) as a function of the number of particles N for four p_a bins.

In this part, we will further explain how TMC affects r_2 and r_3 . Essentially, r_n reflects the ratio of the azimuthal correlation between particles with different momenta to that between particles with the same momenta, i.e., the relationship between $c_n\{2\}|_{p_a, p_b}$, $c_n\{2\}|_{p_a}$, and $c_n\{2\}|_{p_b}$, $r_n = \frac{c_n\{2\}|_{p_a, p_b}}{\sqrt{(c_n\{2\}|_{p_a}) \times (c_n\{2\}|_{p_b})}}$. As can be seen from Eqs. (24) and (28), the analytical result for $c_n\{2\}|_{p_a, p_b}$ is quite complex. Therefore, we need to extract the most critical terms from them as the basis for subsequent analyses. To isolate the influence of TMC, we neglect event-plane fluctuations by assuming $\Psi_n(p_a) = \Psi_n(p_b)$. We have verified that relaxing this assumption does not alter our conclusions, see Appendix C for details. The key terms in $c_2\{2\}$ are given by:

Type I (pure TMC):

$$c_2\{2\}|_{p_a} = \frac{p_a^4}{2(N-2)^2 \langle p^2 \rangle_F^2}, \quad (30)$$

Type II (pure flow + pure TMC):

$$c_2\{2\}|_{p_a} = v_2(p_a)^2 + \frac{p_a^4}{2(N-2)^2 \langle p^2 \rangle_F^2}. \quad (31)$$

In Fig. 3 we compare the results based on Eqs. (30) and (31) with the complete results (labeled as “all”). Here, parameter p_a is taken as the median values within their respective range, while the selection of other parameters is consistent with those in Fig. 1. Figure 3 demonstrates that the “pure TMC + pure flow” contribution accounts for the most of the complete result for all four momentum bins. Therefore, we use the concise “pure TMC + pure flow” result as an efficient proxy for the complete result in the following analysis. Then, r_2 can be rewritten as follows,

$$r_2 = \frac{v_2(p_a)v_2(p_b) + \frac{p_a^2p_b^2}{2(N-2)^2 \langle p^2 \rangle_F^2}}{\sqrt{(v_2(p_a)^2 + \frac{p_a^4}{2(N-2)^2 \langle p^2 \rangle_F^2}) \times (v_2(p_b)^2 + \frac{p_b^4}{2(N-2)^2 \langle p^2 \rangle_F^2})}}. \quad (32)$$

A comparison between Eq. (32) and the complete result is shown in the first row of Fig. 4. We take the results in the low-multiplicity region ($120 \leq N_{\text{ch}} \leq 150$) as an example, since the TMC effect is relatively prominent here, as illustrated in Fig. 1. The excellent agreement between the two results validates the use of this approximation. By the

Cauchy-Schwarz inequality, the expression in Eq. (32) is always less than or equal to 1. This indicates that on top of the pure flow contribution, TMC introduces additional correlations between the azimuthal angles of particles.

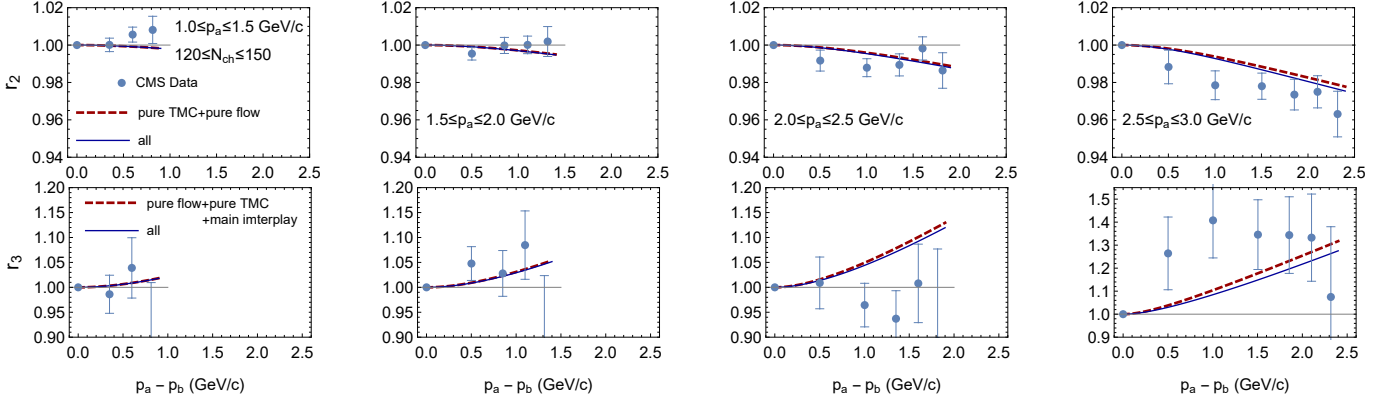


FIG. 4: Factorization ratio r_2 (upper row) and r_3 (lower row) as a function of $p_a - p_b$ in four p_a bins (columns) for $120 \leq N_{ch} \leq 150$. Curves: calculations from TMC and flow (proxy and all). Points: CMS p-Pb data at 5.02 TeV with statistical errors (systematic uncertainties negligible) [41].

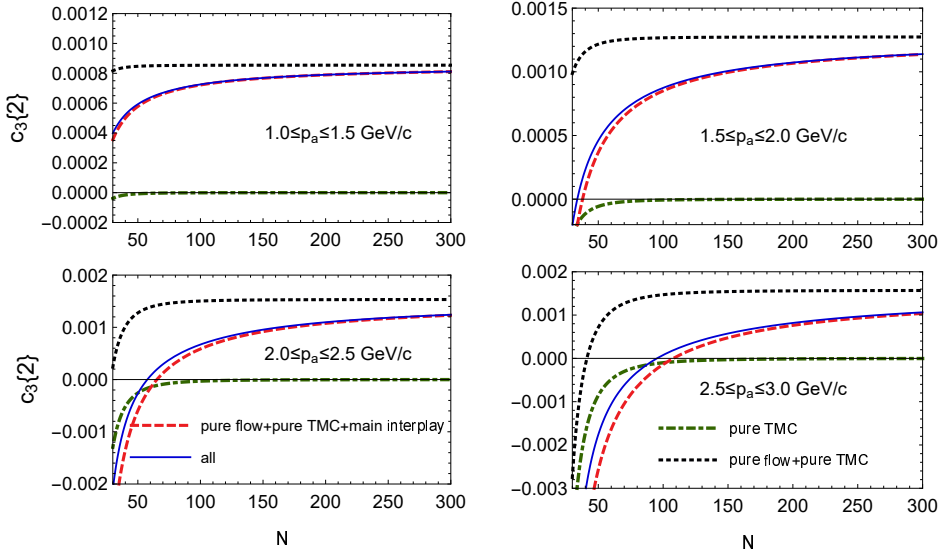


FIG. 5: $c_3 \{2\}$ from “pure TMC”, “pure flow+pure TMC”, “pure flow+pure TMC+main interplay”, and “pure flow+pure TMC+interplay” (labeled “all”) as a function of the number of particles N for four p_a bins.

In a similar way, we obtain and $c_3 \{2\}|_{p_a} r_3$:

Type I (pure TMC):

$$c_3 \{2\}|_{p_a} = -\frac{p_a^6}{6(N-2)^3 \langle p^2 \rangle_F^3}, \quad (33)$$

Type II (pure flow + pure TMC):

$$c_3 \{2\}|_{p_a} = v_3(p_a)^2 - \frac{p_a^6}{6(N-2)^3 \langle p^2 \rangle_F^3}, \quad (34)$$

Type III (pure flow + pure TMC + main interplay):

$$c_3 \{2\}|_{p_a} = v_3(p_a)^2 - \frac{p_a^6}{6(N-2)^3 \langle p^2 \rangle_F^3} - \frac{v_2(p_a)^2 p_a^2 + 2v_3(p_a)^2 p_a^2}{(N-2) \langle p^2 \rangle_F}. \quad (35)$$

Fig. 5 compares the results based on Eqs. (33), (34), and (35) with the complete result, showing that the “pure flow + pure TMC + main interplay” closely reproduces the complete result across broad momentum and multiplicity ranges. Therefore, Eq. (35) will be used as an efficient proxy for the complete result. Then r_3 can be rewritten as follows:

$$r_3 = \frac{v_3(p_a)v_3(p_b) - \frac{p_a^3 p_b^3}{6(N-2)^3 \langle p^2 \rangle_F^3} - \frac{v_2(p_a)v_2(p_b)p_a p_b + v_3(p_a)v_3(p_b)(p_a^2 + p_b^2)}{(N-2)\langle p^2 \rangle_F}}{\sqrt{(v_3(p_a)^2 - \frac{p_a^6}{6(N-2)^3 \langle p^2 \rangle_F^3} - \frac{v_2(p_a)^2 p_a^2 + 2v_3(p_a)^2 p_a^2}{(N-2)\langle p^2 \rangle_F}) \times (v_3(p_b)^2 - \frac{p_b^6}{6(N-2)^3 \langle p^2 \rangle_F^3} - \frac{v_2(p_b)^2 p_b^2 + 2v_3(p_b)^2 p_b^2}{(N-2)\langle p^2 \rangle_F})}}. \quad (36)$$

The second row of Fig. 4 compares the results from Eq. (36) with the complete results, demonstrating their close agreement and thereby validating this substitution. That $r_3 \geq 1$ can be easily proven by a simple mathematical rearrangement of Eq. (36). Physically, pure TMC and the interplay between TMC and flow weakens the 3rd order of azimuthal correlation relative to the pure flow baseline. This weakening is formally shown to be less pronounced for particles with differing momenta than for those with equal momenta. Consequently, the numerator of Eq. (36) becomes larger than the denominator, resulting in $r_3 \geq 1$.

Next, based on the above analysis, we will summarize the general regularity regarding whether TMC causes r_n to be greater than 1 or less than 1. For the two-particle correlation cumulants of any order, namely $c_n\{2\}$, we can divide their analytical results into three categories: pure TMC, pure flow, and their interplay term. The three categories contribute hierarchically: pure TMC reflects the variation trend of $c_n\{2\}$ with multiplicity; pure flow adjusts the sign and order of magnitude of $c_n\{2\}$ on the basis of pure TMC; and the interplay term further fine-tunes the numerical value based on the previous two. Therefore, the pure TMC and pure flow contributions capture the essential variation trends and order of magnitude of $c_n\{2\}$. This justifies our subsequent analysis of r_n , which will be framed in terms of these two dominant components. For $c_n\{2\}|_{p_a, p_b}$, the specific form of pure flow is always $v_n(p_a)v_n(p_b)$. Next, we derive the general formula for pure TMC. That is, without considering v_n , the calculation of $c_n\{2\}|_{p_a, p_b}$ is as follows:

$$c_n\{2\}|_{p_a, p_b} = \left\langle e^{in(\phi_1^a - \phi_2^b)} \right\rangle = \frac{\int_0^{2\pi} e^{in(\phi_1^a - \phi_2^b)} \exp(X) d\phi_1^a d\phi_2^b}{\int_0^{2\pi} \exp(X) d\phi_1^a d\phi_2^b}, \quad (37)$$

where, according to Eq. (15), the form of X is as follows:

$$X = -\frac{2p_a p_b \cos(\phi_1^a - \phi_2^b)}{(N-2)\langle p^2 \rangle_F}. \quad (38)$$

We still perform a Taylor expansion on the exponential term in Eq. (38), i.e., $\exp(X) = 1 + X + \frac{X^2}{2} + \frac{X^3}{6} + \dots$, expanding until the first non-zero result appears. However, for the denominator, we only take the first term of its expansion, so the result is $(2\pi)^2$. Therefore, the general formula for pure TMC is $(-1)^n \frac{1}{n!} \frac{p_a^n p_b^n}{(N-2)^n \langle p^2 \rangle_F^n}$. Then, r_n can be written in the following form (this serves as a useful approximation that, while not exact, reproduces the key features.):

$$r_n = \frac{v_n(p_a)v_n(p_b) + (-1)^n \frac{1}{n!} \frac{p_a^n p_b^n}{(N-2)^n \langle p^2 \rangle_F^n}}{\sqrt{(v_n(p_a)^2 + (-1)^n \frac{1}{n!} \frac{p_a^{2n}}{(N-2)^n \langle p^2 \rangle_F^n}) \times (v_n(p_b)^2 + (-1)^n \frac{1}{n!} \frac{p_b^{2n}}{(N-2)^n \langle p^2 \rangle_F^n})}}. \quad (39)$$

From Eq. (39), it can be seen that without the TMC effect, $r_n = \frac{v_n(p_a)v_n(p_b)}{\sqrt{v_n(p_a)^2 v_n(p_b)^2}} = 1$. However, the introduction of the TMC effect will change the azimuthal correlation of two particles. Next, squaring both the numerator and denominator of Eq. (39) allows for a direct observation of the TMC contribution.

The result of squaring the numerator of Eq. (39) is as follows:

$$\begin{aligned} U &= v_n(p_a)^2 v_n(p_b)^2 + \frac{1}{(n!)^2} \frac{p_a^{2n} p_b^{2n}}{(N-2)^{2n} \langle p^2 \rangle_F^{2n}} + 2v_n(p_a)v_n(p_b)(-1)^n \frac{1}{n!} \frac{p_a^n p_b^n}{(N-2)^n \langle p^2 \rangle_F^n} \\ &= U_1 + U_2 + U_3, \end{aligned} \quad (40)$$

where the sum of the second and third terms ($U_2 + U_3$) in Eq. (40) are the changes in the azimuthal correlation of two particles with different momenta caused by the introduction of TMC.

The result of squaring the denominator of Eq. (39) is as follows:

$$D = v_n (p_a)^2 v_n (p_b)^2 + \frac{1}{(n!)^2} \frac{p_a^{2n} p_b^{2n}}{(N-2)^{2n} \langle p^2 \rangle_F^{2n}} + v_n (p_a)^2 (-1)^n \frac{1}{n!} \frac{p_b^{2n}}{(N-2)^n \langle p^2 \rangle_F^n} + v_n (p_b)^2 (-1)^n \frac{1}{n!} \frac{p_a^{2n}}{(N-2)^n \langle p^2 \rangle_F^n}$$

$$= D_1 + D_2 + D_3 + D_4, \quad (41)$$

where the sum of the second, third, and fourth terms ($D_2 + D_3 + D_4$) in Eq. (41) are the changes in the azimuthal correlation of two particles with the same momentum caused by the introduction of TMC. Since $D_2 = U_2$, the comparison of the TMC effect between particles with different momenta and those with the same momentum reduces to comparing U_3 to $D_3 + D_4$. According to the mean inequality, $A + B \geq 2\sqrt{AB}$ (where $A \geq 0$ and $B \geq 0$), we have:

$$\begin{cases} D_3 + D_4 \geq 2\sqrt{D_3 D_4} = U_3, & \text{if } n = 2k, k \in \mathbb{N}^+, \\ D_3 + D_4 \leq U_3, & \text{if } n = 2k + 1, k \in \mathbb{N}^+. \end{cases} \quad (42)$$

Thus, for the factorization ratio r_n we have:

$$\begin{cases} r_n \leq 1, & \text{if } n = 2k, k \in \mathbb{N}^+, \\ r_n \geq 1, & \text{if } n = 2k + 1, k \in \mathbb{N}^+. \end{cases} \quad (43)$$

This is due to the weaker influence of TMC on the azimuthal correlation for particle pairs with different momenta compared to those with identical momenta, i.e., $|U_3| \leq |D_3 + D_4|$. Consequently, the TMC causes r_n to deviate from unity; the sign of this deviation (whether $r_n > 1$ or $r_n < 1$) is determined by whether the pure TMC contributes positively or negatively to the two-particle azimuthal correlations of different orders. We find that the sign of the pure TMC contribution to $c_n \{2\}$ alternates with the harmonic order n as $(-1)^n$. Note that this method is only used to quickly judge the relationship between r_n and 1, and cannot be used as an accurate numerical replacement. For example, for r_3 , an accurate replacement of the complete result must also take into account the impact of the interplay. Additionally, we have also verified r_4 , and the complete result is indeed less than 1.

IV. CONCLUSIONS

In this paper, we calculate factorization ratios r_2 and r_3 of two-particle azimuthal correlations as a function of $p_a - p_b$ under the constraint of transverse momentum conservation. We observe that the TMC effect causes both r_2 and r_3 to deviate from 1, with the deviation increasing as the momentum difference between particles grows. Physically, the TMC alters azimuthal two-particle correlations relative to the pure flow baseline, applying a smaller correction to pairs with differing momenta than to those with the same momentum. By introducing a positive correlation to $c_2 \{2\}$ but a negative one to $c_3 \{2\}$, the TMC leads to $r_2 \leq 1$ and $r_3 \geq 1$. In addition, it can also be seen that our analytical results for r_2 and r_3 both show the most significant deviation from 1 at low multiplicities and high momenta, which reflects the characteristics of TMC. Our analytical results are in good agreement with the CMS p-Pb data for both r_2 and r_3 within errors. Therefore, the TMC effect must be included as an essential physical component in interpreting these experimental results. Finally we find that within the TMC framework, the factorization ratio obeys $r_n < 1$ for even n and $r_n > 1$ for odd n . This stems from the sign-alternating pure TMC contribution to $c_n \{2\}$, which is proportional to $(-1)^n$. A promising direction for future work is to generalize the framework and include the longitudinal momentum conservation. This would enable a comprehensive study of its role in driving longitudinal decorrelation, ultimately clarifying the emergent correlation dynamics in the full phase space of small systems.

ACKNOWLEDGMENTS

This work is partially supported by the National Natural Science Foundation of China under Grants No. 12325507, No. 12547102, and No. 12147101, and the National Key Research and Development Program of China under Grant No. 2022YFA1604900 (J.P. and G.M.), the Ministry of Science and Higher Education (PL), and the National Science Centre (PL), Grant No. 2023/51/B/ST2/01625 (A.B.).

APPENDIX

A. $v_n(p)$

To compare our results with the data, we need to determine the dependence of elliptic flow parameter v_2 on transverse momentum p . Since CMS has measured the data of $v_2\{2\}$ and $v_2\{4\}$ as functions of p under different multiplicities N_{ch} in p-Pb collisions at 5.02 TeV, we will determine $v_2(p)$ based on them [57]. Fluctuations in the elliptic flow v_2 are driven by event-by-event differences in the initial geometry, including impact parameter and participant nucleon positions. The fluctuation of v_2 can be defined as follows [59],

$$\sigma^2 = \langle v_2^2 \rangle - \langle v_2 \rangle^2. \quad (\text{A.1})$$

We consider how fluctuations affect the flow observable $f(v_2)$. When the function $f(v_2)$ is expanded in a series around the average value of the collective flow $\langle v_2 \rangle$ up to the second-order term, the average value of the collective flow observable $f(v_2)$, denoted as $\langle f(v_2) \rangle$, is:

$$\langle f(v_2) \rangle = f(\langle v_2 \rangle) + \frac{\sigma^2}{2} f''(\langle v_2 \rangle). \quad (\text{A.2})$$

Therefore, based on Eqs. (A.1) and (A.2), we can respectively derive the collective flows $v_2\{2\}$ and $v_2\{4\}$ measured via two-particle correlations and four-particle correlations:

$$v_2\{2\}^2 = \langle v_2^2 \rangle = \langle v_2 \rangle^2 + \sigma^2, \quad (\text{A.3})$$

$$v_2\{4\}^2 = \left(2 \langle v_2^2 \rangle^2 - \langle v_2^4 \rangle \right)^{\frac{1}{2}} \approx \langle v_2 \rangle^2 - \sigma^2. \quad (\text{A.4})$$

By combining Eqs. (A.3) and (A.4), the fluctuations can be eliminated to obtain $\langle v_2 \rangle$:

$$\langle v_2 \rangle = \sqrt{\frac{v_2\{2\}^2 + v_2\{4\}^2}{2}}. \quad (\text{A.5})$$

We perform a polynomial fit to the experimental data. The specific fitting formulas are given in Table I and a comparison between the fitting results and the data is shown in Fig. 6. Here, under the same experimental conditions for triangular flow v_3 , only two-particle correlation data are available, and the value in parentheses is the coefficient of determination, R^2 :

TABLE I: Polynomial fits to the p_T -dependence of $v_2\{2\}$, $v_2\{4\}$, and $v_3\{2\}$ in four N_{ch} ranges for p-Pb collisions at 5.02 TeV.

N_{ch}	$v_2\{2\}$	$v_2\{4\}$	$v_3\{2\}$
$220 \leq N_{ch} \leq 260$	$0.0832p - 0.0105p^2$ (0.991)	$0.062p - 0.008p^2 - 0.00064p^3 + 0.0001p^4$ (0.998)	$0.036p - 0.0056p^2$ (0.943)
$185 \leq N_{ch} \leq 220$	$0.0827p - 0.0101p^2$ (0.993)	$0.054p + 0.003p^2 - 0.005p^3 + 0.0005p^4$ (0.998)	$0.034p - 0.0055p^2$ (0.943)
$150 \leq N_{ch} \leq 185$	$0.0823p - 0.01p^2$ (0.99)	$0.061p + 0.001p^2 - 0.005p^3 + 0.0006p^4$ (0.996)	$0.035p - 0.0064p^2$ (0.977)
$120 \leq N_{ch} \leq 150$	$0.0818p - 0.0097p^2$ (0.991)	$0.057p + 0.002p^2 - 0.006p^3 + 0.0006p^4$ (0.997)	$0.03p - 0.0059p^2$ (0.944)

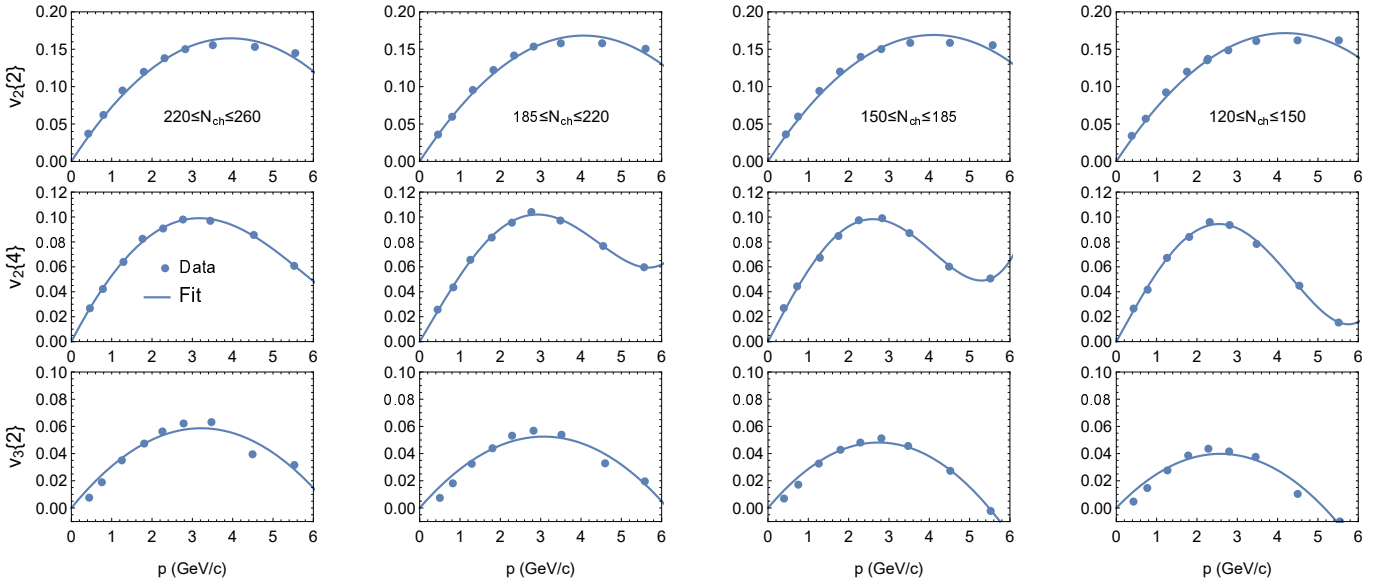


FIG. 6: Central values of $v_2\{2\}$ (upper row), $v_2\{4\}$ (middle row), and $v_3\{2\}$ (lower row) as a function of transverse momentum p in four N_{ch} ranges (columns) in p-Pb collisions at $\sqrt{s_{NN}} = 5.02$ TeV from the CMS experiment [57]. The curves represent polynomial fits to the experimental data.

B. $\cos[n\Psi_n(p_a) - n\Psi_n(p_b)]$

Here we perform a polynomial fit to the experimental data of r_2 under high multiplicities. The specific fitting formulas are as follows:

$2.0 \leq p_a \leq 2.5$ GeV/c:

$$\cos[2\Psi_2(p_a) - 2\Psi_2(p_b)] \approx r_2 \approx 0.998 - 0.005 \times (p_a - p_b), \quad (\text{B.1})$$

$2.5 \leq p_a \leq 3.0$ GeV/c:

$$\cos[2\Psi_2(p_a) - 2\Psi_2(p_b)] \approx r_2 \approx 1 - 0.012 \times (p_a - p_b). \quad (\text{B.2})$$

For r_2 at the remaining p_a momentum bins and for r_3 at all p_a momentum bins, the data are consistent with unity within experimental uncertainties. Therefore, for simplicity, we set these event-plane correlations to a value of 1 in our analysis. A comparison between the curves for Eqs. (B.1), (B.2), and the experimental data is shown in Fig. 7. Here, we adopt the simplest possible fit that is consistent with the experimental uncertainties while reproducing the general trend of the data.

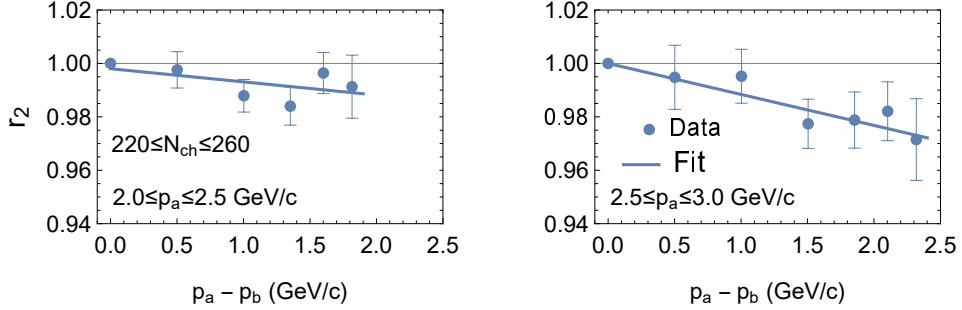


FIG. 7: Factorization ratio r_2 as a function of $p_a - p_b$ in two p_a bins for high N_{ch} range of $220 \leq N_{ch} \leq 260$ in p-Pb collisions at $\sqrt{s_{NN}} = 5.02$ TeV from the CMS experiment [41]. The curves represent polynomial fits to the experimental data.

C. r_2 and r_3 without considering p_T -dependent event plane fluctuations

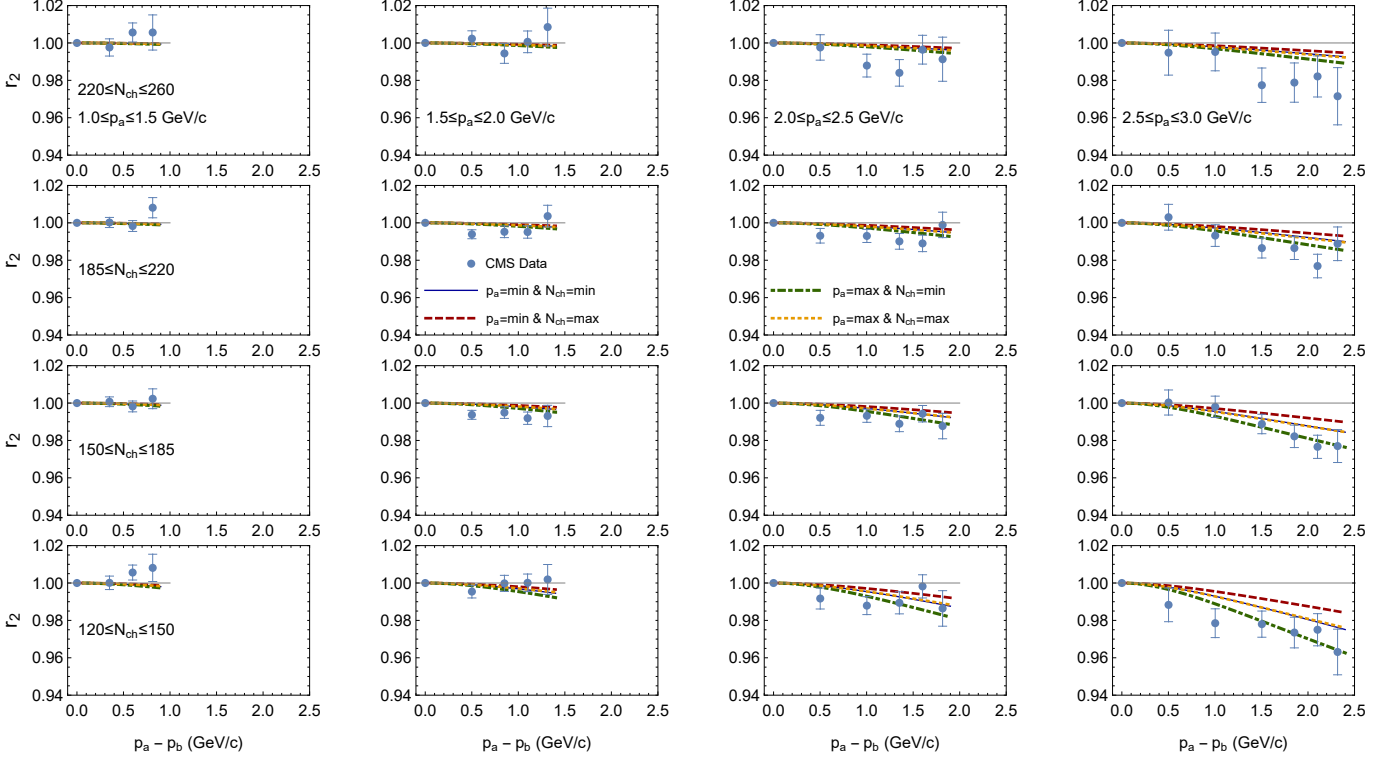
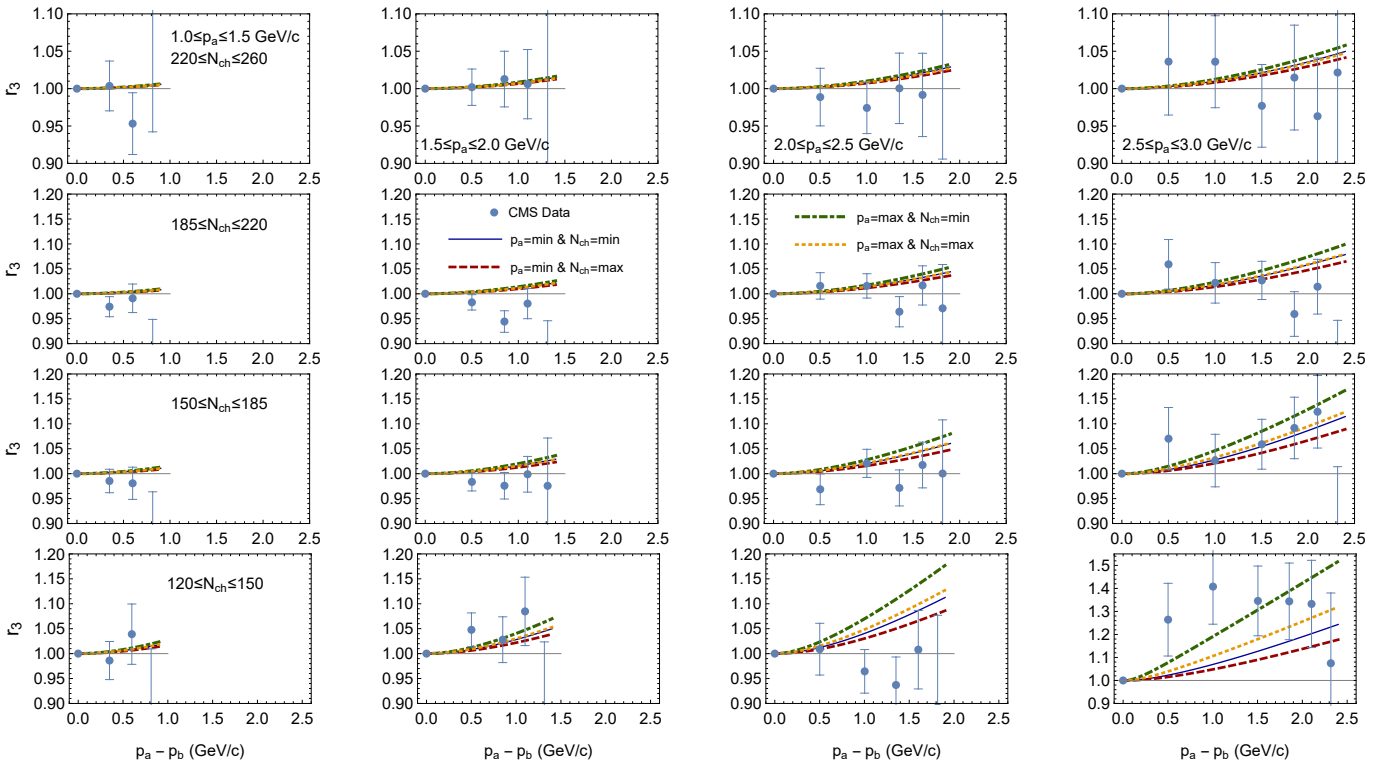


FIG. 8: Same as Fig. 1, but without considering p_T -dependent event plane fluctuations.

Figures 8 and 9 show the results obtained by assuming a common event plane for all p_T bins. Although this neglects event-plane fluctuations, we find that both the quality of the fits and our key conclusions remain robust, compared to Figs. 1 and 2. Compared with Fig. 1, the curves in Fig. 8 are slightly elevated. However, Fig. 9 is virtually identical to Fig. 2, indicating that r_3 is insensitive to fluctuations in the second-order event plane.

FIG. 9: Same as Fig. 2, but without considering p_T -dependent Ψ_2 fluctuations.

[1] B. B. Back et al. (PHOBOS), Nucl. Phys. A **757**, 28 (2005), nucl-ex/0410022.

[2] J. Chen et al., Nucl. Sci. Tech. **35**, 214 (2024), 2407.02935.

[3] I. Arsene et al. (BRAHMS), Nucl. Phys. A **757**, 1 (2005), nucl-ex/0410020.

[4] J. Adams et al. (STAR), Nucl. Phys. A **757**, 102 (2005), nucl-ex/0501009.

[5] J.-H. Chen, J. Chen, F.-K. Guo, Y.-G. Ma, C.-P. Shen, Q.-Y. Shou, Q. Shou, Q. Wang, J.-J. Wu, and B.-S. Zou, Nucl. Sci. Tech. **36**, 55 (2025), 2411.18257.

[6] J.-Y. Ollitrault, Phys. Rev. D **46**, 229 (1992).

[7] J. Adams et al. (STAR), Phys. Rev. Lett. **92**, 052302 (2004), nucl-ex/0306007.

[8] G. Aad et al. (ATLAS), Phys. Lett. B **707**, 330 (2012), 1108.6018.

[9] S. Chatrchyan et al. (CMS), Phys. Rev. C **87**, 014902 (2013), 1204.1409.

[10] S. A. Voloshin, A. M. Poskanzer, and R. Snellings, Landolt-Bornstein **23**, 293 (2010), 0809.2949.

[11] U. Heinz and R. Snellings, Ann. Rev. Nucl. Part. Sci. **63**, 123 (2013), 1301.2826.

[12] C. Gale, S. Jeon, and B. Schenke, Int. J. Mod. Phys. A **28**, 1340011 (2013), 1301.5893.

[13] Z.-W. Lin, C. M. Ko, B.-A. Li, B. Zhang, and S. Pal, Phys. Rev. C **72**, 064901 (2005), nucl-th/0411110.

[14] S. Voloshin and Y. Zhang, Z. Phys. C **70**, 665 (1996), hep-ph/9407282.

[15] A. M. Poskanzer and S. A. Voloshin, Phys. Rev. C **58**, 1671 (1998), nucl-ex/9805001.

[16] J. Jia et al., Nucl. Sci. Tech. **35**, 220 (2024), 2209.11042.

[17] B. Alver and G. Roland, Phys. Rev. C **81**, 054905 (2010), [Erratum: Phys. Rev. C 82, 039903 (2010)], 1003.0194.

[18] B. H. Alver, C. Gombeaud, M. Luzum, and J.-Y. Ollitrault, Phys. Rev. C **82**, 034913 (2010), 1007.5469.

[19] M. Luzum, Phys. Lett. B **696**, 499 (2011), 1011.5773.

[20] J.-f. Wang, H.-j. Xu, and F.-Q. Wang, Nucl. Sci. Tech. **35**, 108 (2024), 2305.17114.

[21] C. Gale, S. Jeon, B. Schenke, P. Tribedy, and R. Venugopalan, Phys. Rev. Lett. **110**, 012302 (2013), 1209.6330.

[22] D. Teaney and L. Yan, Phys. Rev. C **90**, 024902 (2014), 1312.3689.

[23] D. Everett et al. (JETSCAPE), Phys. Rev. C **103**, 054904 (2021), 2011.01430.

[24] G. Nijs, W. van der Schee, U. Gürsoy, and R. Snellings, Phys. Rev. C **103**, 054909 (2021), 2010.15134.

[25] M. Luzum and H. Petersen, J. Phys. G **41**, 063102 (2014), 1312.5503.

[26] H. Song, Y. Zhou, and K. Gajdosova, Nucl. Sci. Tech. **28**, 99 (2017), 1703.00670.

[27] Q.-Y. Shou et al., Nucl. Sci. Tech. **35**, 219 (2024), 2409.17964.

[28] P. Danielewicz and G. Odyniec, Phys. Lett. B **157**, 146 (1985), 2109.05308.

- [29] S. Chatrchyan et al. (CMS), JHEP **02**, 088 (2014), 1312.1845.
- [30] F. G. Gardim, F. Grassi, M. Luzum, and J.-Y. Ollitrault, Phys. Rev. C **87**, 031901 (2013), 1211.0989.
- [31] U. Heinz, Z. Qiu, and C. Shen, Phys. Rev. C **87**, 034913 (2013), 1302.3535.
- [32] A. Dumitru, K. Dusling, F. Gelis, J. Jalilian-Marian, T. Lappi, and R. Venugopalan, Phys. Lett. B **697**, 21 (2011), 1009.5295.
- [33] K. Dusling and R. Venugopalan, Phys. Rev. D **87**, 094034 (2013), 1302.7018.
- [34] V. Skokov, Phys. Rev. D **91**, 054014 (2015), 1412.5191.
- [35] E. Shuryak and I. Zahed, Phys. Rev. C **88**, 044915 (2013), 1301.4470.
- [36] A. Bzdak, B. Schenke, P. Tribedy, and R. Venugopalan, Phys. Rev. C **87**, 064906 (2013), 1304.3403.
- [37] G.-Y. Qin and B. Müller, Phys. Rev. C **89**, 044902 (2014), 1306.3439.
- [38] G.-L. Ma and A. Bzdak, Phys. Lett. B **739**, 209 (2014), 1404.4129.
- [39] A. Bzdak and G.-L. Ma, Phys. Rev. Lett. **113**, 252301 (2014), 1406.2804.
- [40] D.-F. Wang, M.-Y. Chen, Y.-G. Ma, Q.-Y. Shou, S. Zhang, and L. Zheng, Nucl. Sci. Tech. **36**, 154 (2025), 2501.15776.
- [41] V. Khachatryan et al. (CMS), Phys. Rev. C **92**, 034911 (2015), 1503.01692.
- [42] E. G. Nielsen and Y. Zhou, Eur. Phys. J. C **83**, 545 (2023), 2211.13651.
- [43] J. L. Nagle and W. A. Zajc, Ann. Rev. Nucl. Part. Sci. **68**, 211 (2018), 1801.03477.
- [44] N. Borghini, P. M. Dinh, and J.-Y. Ollitrault, Phys. Rev. C **62**, 034902 (2000), nucl-th/0004026.
- [45] Z. Chajecki and M. Lisa, Phys. Rev. C **78**, 064903 (2008), 0803.0022.
- [46] S. Pratt, S. Schlichting, and S. Gavin, Phys. Rev. C **84**, 024909 (2011), 1011.6053.
- [47] A. Bzdak and G.-L. Ma, Phys. Rev. C **97**, 014903 (2018), 1710.00653.
- [48] A. Bzdak and G.-L. Ma, Phys. Lett. B **781**, 117 (2018), 1801.01277.
- [49] M.-T. Xie, G.-L. Ma, and A. Bzdak, Phys. Rev. C **105**, 054904 (2022), 2204.01038.
- [50] J.-L. Pei, G.-L. Ma, and A. Bzdak, Phys. Rev. C **110**, 024901 (2024), 2403.05782.
- [51] J.-L. Pei, G.-L. Ma, and A. Bzdak, Phys. Rev. C **112**, 034909 (2025), 2503.12846.
- [52] S. Acharya et al. (ALICE), JHEP **09**, 032 (2017), 1707.05690.
- [53] K. Aamodt et al. (ALICE), Phys. Rev. Lett. **107**, 032301 (2011), 1105.3865.
- [54] N. Borghini, Eur. Phys. J. C **30**, 381 (2003), hep-ph/0302139.
- [55] A. Bzdak, V. Koch, and J. Liao, Phys. Rev. C **83**, 014905 (2011), 1008.4919.
- [56] Z. Chajecki and M. Lisa, Phys. Rev. C **79**, 034908 (2009), 0807.3569.
- [57] S. Chatrchyan et al. (CMS), Phys. Lett. B **724**, 213 (2013), 1305.0609.
- [58] B. B. Abelev et al. (ALICE), Phys. Lett. B **727**, 371 (2013), 1307.1094.
- [59] J. Adams et al. (STAR), Phys. Rev. C **72**, 014904 (2005), nucl-ex/0409033.